Available online at http://www.journalcra.com

International Journal of Current Research
Vol. 10, Issue, 06, pp.70066-70073, June, 2018

INTERNATIONAL JOURNAL OF CURRENT RESEARCH

ISSN: 0975-833X

RESEARCH ARTICLE

STRUCTURAL AND MAGNETIC PROPERTIES OF Nb-Zn DOPED BARIUM STRONTIUM HEXAFERRITE NANOCOMPOSITE POWDER PREPARED BY SOL-GEL METHOD

[1]Gayathri, S., [2,]*S. Jesurani, [3]Ashok K. and [4]John Peter, A.

[1,2] PG and Research Department of Physics, Jayaraj Annapackiam College for Women (autonomous) Periyakulam- 625601, Tamilnadu, India.
[3]Materials and Mechanical Entity, Vikram Sarabhai Space Centre (ISRO), Thiruvananthapuram-695022, Kerala, India
[4]P.G and Research Dept.of Physics, Government Arts College, Melur-625 106 Madurai India

ARTICLE INFO

Article History:
Received 14th March, 2018
Received in revised form
27th April, 2018
Accepted 20th May, 2018
Published online 28th June, 2018

Key words:
Barium Strontium Hexaferrite,
Sol-gel, Structural Properties,
Magnetic Properties.

ABSTRACT

M-type hexagonal ferrites with chemical composition $Ba_{0.5}Sr_{0.5}Fe_{12-2x}Nb_xZn_xO_{19}$(X=0, 0.05, 0.1, 0.25, 0.5 mol %) have been synthesized by sol-gel method using D- glucose as fuel. In the present work, Barium, Strontium, Iron, Zinc nitrate, Niobium chloride are used raw materials and D-glucose was used as fuel. The prepared samples were calcined at 800^0C and 950^0C. TGA/DTA curve shows there is no weight loss above 850^0C which confirmed the formation of barium strontium hexaferrite. FTIR spectra exhibit the band in the range of 453– 495cm^{-1} which revealed the presence of hexagonal ferrite. The phase formations were investigated by X-ray diffraction. X-ray powder analysis confirmed the formation of hexagonal magnetoplumbite structure. The average particle size of the sample is in the range of 31- 48 nm. SEM micrographs showed the powder is well crystallized and the particles are hexagonal structure with needle shape and platelet form. EDAX analysis showed the evidence for the presence of Ba, Sr, Fe, Nb and Zn. The VSM measurement revealed that the doping of Nb-Zn ions caused the change in the magnetic properties such as coercivity, saturation magnetization and remanence magnetization. The improving saturation magnetization and remanence magnetization and reducing coercivity were favorable for high density perpendicular magnetic recording applications.

Corresponding author:

Citation: Gayathri, S., S. Jesurani, Ashok K. and John Peter, A., 2018. "Structural and magnetic properties of nb-zn doped barium strontium hexaferrite nanocomposite powder prepared by sol-gel method", *International Journal of Current Research*, 10, (06), 70066-70073.

INTRODUCTION

Permanently magnetizable materials acquire great scientific, industrial and technological interests due to their crucial role in the fabrication of essential components for multitude of devices and machines in active uses nowadays. M-type hexaferrite ($MFe_{12}O_{19}$, M= Ba, Sr, Pb) are extensively used as permanent magnets, high density magnetic recording media and microwave devices due to their large saturation magnetization, high coercivity, high curie temperature, good chemical stability, corrosion resistance and unsurpassed low cost (Yang Yujie, 2018). Ba-Sr hexaferrite powders with the doping of different ions are extensively studied for the development of materials for magnetic recording media and electromagnetic attenuation due to their low density, large electrical resistivity and microwave absorption purposes (Waseem Abbas *et al*., 2015).

In order to prepare hexaferrite particles, several synthesizing techniques have been developed such as the solid state method (Marin Cernea, 2013), ceramic process (Yujie Yang, 2017), co–precipitated method (Muhammad, 2010), conventional ceramic route (Mozaffari, 2010), mechano-chemical method (Winataputra, 2017), sol-gel method (Kanagesan, 2012) and citrate gel combustion method (Ezhil Vizhi, 2016). Sr-Ba based hexaferrites are investigated by many researchers due to their novel application (Fuzhan Song *et al*., 2010). It is well known that there are five distinct crystallographic sites or sublattices for the cations: three octahedral (2a, 12k, $4f_2$), one tetrahedral ($4f_1$) and one trigonal bipyramidal (2b) in a unit cell of M-type hexaferrite. The spin directions for the 2a,12k and 2b sublattices are parallel to each other (in the direction of the crystallographic c-axis), in which $4f_1$ and $4f_2$ sublattices are in the opposite direction which are coupled by super exchange interaction through the o^{2-} ions and form the ferromagnetic structure.

The cations on different sites make different contributions to the magnetic properties of the ferrites (Kanagesan *et al*., 2014). Many researchers pointed out that the magnetic properties of substituted M-type hexaferrite which has been considered suitable for different applications and are strongly dependent on the occupation of the sites by different cations. Several cations such as La^{3+}(Thakur, 2013), Ce^{3+}(Pawar *et al*., 2015), Pr^{3+}(Abbas *et al*., 2015), Sm^{3+}(Buzinaro, 2016), Nd^{3+} (Mocuta *et al*., ?), Co^{2+}(Chavan *et al*., 2016), Ti^{4+}(Mariño-Castellanos, 2004), In^{3+}(Trukhanov *et al*., 2016), Bi^{3+}(Auwal *et al*., 2016), Al^{3+}(Trukhanov *et al*., 2015), Cr^{3+}(Dhage, 2013), Cu^{2+}(Awadallah *et al*., 2016)and Mn^{2+}(Silva, 2015), have been reported . M-type hexaferrite has been shown with the combination of substitution with La-Co (Wangchang *et al*., 2013) and Co-Al (Jasbir Singh *et al*., 2016). Kanagesan *et al*., synthesized Zn-Nb substituted nanocrystalline barium hexaferrite $BaFe_{12-2x}Zn_xNb_xO_{19}$ (X=0.2, 0.4, 0.6, 0.8 mol %) by sol-gel method and found that the saturation magnetization and coercivity increase with increasing Zn-Nb concentration. Nb-Zn substituted Barium Strontium hexaferrite is a new kind of very promising particulate material for magnetic recording (Samikannu Kanagesan, 2014). In the present work, Nb-Zn doped M- type hexaferrite $Ba_{0.5}Sr_{0.5}Fe_{12-2x}Nb_xZn_xO_{19}$ (X = 0 to 0.5 mol %) are prepared by the sol-gel method. The structural and magnetic properties of Nb-Zn doped M-type Barium Strontium hexaferrite are investigated.

MATERIALS AND METHODS

The $Ba_{0.5}Sr_{0.5}Fe_{12-2x}Nb_xZn_xO_{19}$ nanocomposite powder was prepared by sol-gel method using D-glucose as fuel. Analytical reagent grade $Ba(No_2)_3$, $Sr(No_2)_3$, $Fe(NO_3).9H_2O$, $Zn(NO_2)_3$, $NbCl_5$ and D- glucose were used as staring materials. According to the composition of $Ba_{0.5}Sr_{0.5}Fe_{12-2x}Nb_xZn_xO_{19}$ (X = 0, 0.05, 0.1, 0.25, 0.5 mol %) all the nitrates were separately dissolved in a minimum amount of distilled water and stirred on a magnetic stirrer for 15 minutes. All the solutions were mixed together and stirred on a magnetic stirrer until the nitrates were completely dissolved. The metal nitrates and D-glucose in the molar ratio of 1:1 were dissolved in distilled water to obtain an aqueous solution using magnetic stirrer and then added 4ml of ethylene glycol which acts as reducing agent and finally gelling agent is added. The resultant solution was stirred continuously and heated up to 80^0C to obtain a sticky liquid gel. The gel was heated in a hot air oven at 110^0C for 24 hours to get precursor powder which was used to take FTIR and TGA/DTA. The resulting nanocomposite powder was calcined at two different temperatures 800^0C and 950^0C for 3 hours to obtain $Ba_{0.5}Sr_{0.5}Fe_{12-2x}Nb_xZn_xO_{19}$ powder which is used for XRD, SEM, EDAX and VSM characterizations.

Measurements and characterization: The prepared $Ba_{0.5}Sr_{0.5}Fe_{12-2x}Nb_xZn_xO_{19}$ samples in a nanosize form were characterized by standard techniques such as thermo gravimetric analysis (TGA/DTA), Fourier transform infrared spectroscopy (FTIR), X-ray diffraction (XRD), Scanning electron microscope (SEM), EDAX (Energy dispersive X-ray spectroscopy) and Vibrating sample magnetometer (VSM). The precursor is used to take TG/DTA under instrument SDT Q600 V8.3 Build 101.R. Fourier transform infrared spectroscopy (FTIR) of the prepared samples were recorded in the region of 4000-400 cm^{-1} on PerkinElmer spectrum-100 spectrometer using KBr as a reference material. The XRD (PANalytical X'Pert pro diffract to meter) patterns were recorded at room temperature in the range of 10^0C to 20^0C using Cu- Kα radiation (λ =1.54060 A^0). SEM technique (model JEOL JSM-6360) was used to study the surface morphology of the samples and also particle size of the sample. The magnetic properties were measured at room temperature with the vibrating sample magnetometer (Lakeshore 7304 model).

RESULTS AND DISCUSSION

Thermal analysis: The sample was monitored by thermogravimetric analysis (TGA) and differential thermal analysis (DTA). Fig 2 reflects the TGA/DTA curves of the undoped sample of $BaSrFe_{12}O_{19}$ with the heating rate at 10^0C /min in air. The thermal analysis shows the formation of hexaferrite phase. The first weight loss was observed at about 25^0C-150^0C which represents the loss of residual water from the powdered surface. The next weight loss was obtained in the range of 400^0C - 800^0C due to the decomposition of the hydroxides of barium, strontium, iron into corresponding metal oxides. In the DTA curve, two distinct exothermic peaks between 200^0C and 400^0C are due to the decomposition of D-glucose and one endothermic peak around 576^0C may be the decomposition of the residual amorphous carbon. From the results, it is clear that the dry glucose burns drastically after absorbing some energy and then gives out great quantity of heat. The exothermic, endothermic and weight loss at temperature between 200^0C to 800^0C can be assigned to the starting formation of monoferrite and hexaferrite and there is no noticeable weight loss above 850^0C which confirmed the formation of barium strontium hexaferrite. The crystalline temperature attained above 850^0C due to the addition of fuel (D–glucose) (Awadallah *et al*., 2016).

FTIR spectra study: The FTIR spectra of the prepared sample of precursors are shown in fig 3. FTIR Spectra are in the range of 4000-400 cm^{-1} for the sample with different concentrations. The largest absorption band around 3451 to 3498 cm^{-1} is attributed to the stretching of water molecules in the band of O=H . The strongest absorption band is observed between the wave number 1704 and 1724 cm^{-1} corresponding stretching of vibration C=O. Another band was located at the wave number 1353-1381 cm^{-1} in the bending of nitro groups. The small absorption bands are assigned to C- O stretching of 1010-1065cm^{-1}. The sharp absorption peak 797 cm^{-1} belongs to metal oxide stretching of vibration. The bands around 453 to 495 cm^{-1} are characteristic peaks which confirmed the presence of hexaferrite. The FTIR spectra showed different functional groups of barium strontium hexaferrite with doping of Nb-Zn nanocomposition (Safia Anjum *et al*., 2016).

Structural Analysis: XRD analysis was carried out for the investigation of crystal structure of the prepared samples. Fig 4a and 4b show the XRD patterns of $Ba_{0.5}Sr_{0.5}Fe_{12-2x}Nb_xZn_xO_{19}$ (X=0, 0.05, 0.1, 0.25, 0.5 mol %) samples prepared by sol-gel method and then these samples were calcined at two various temperatures (800^0C and 950^0C). The XRD patterns were recorded at room temperature in the range of 10^0C to 80^0C using Cu-Kα radiation (1.54060A^0).The observed peaks are sharp and well defined which reflect that prepared samples are well crystallized. The XRD patterns were indexed to hexagonal magnetoplumbite (M-type) structure having space group $P6_3/mmc$ (JCPDS file no: 51-1879) and a small fraction of secondary phase (α-Fe_2O_3) was also present. The lattice constants and c were calculated using the following formula (Yang Yujie *et al*., 2018).

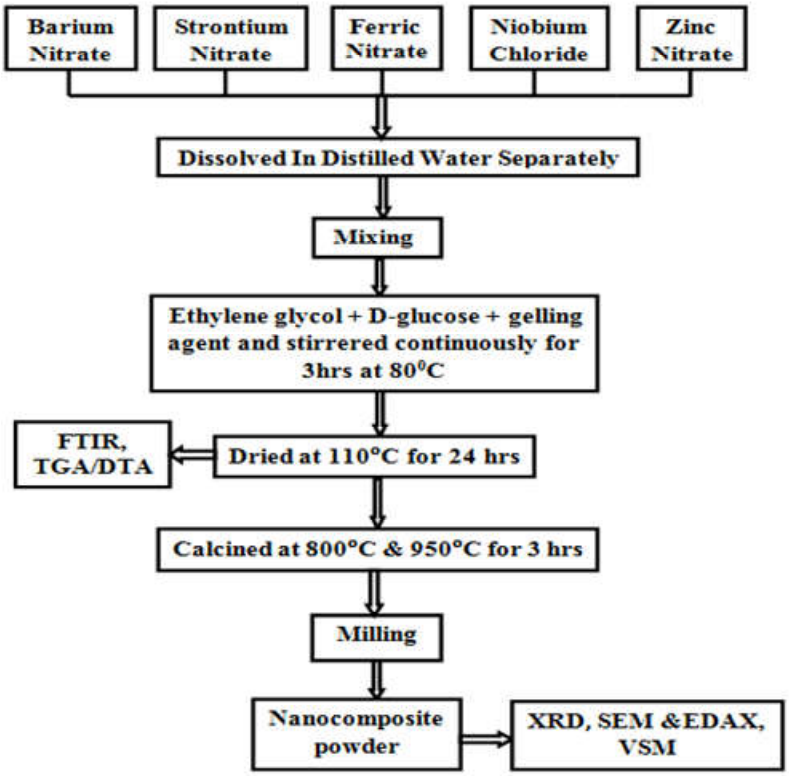

Fig. 1. Flowchart of synthesis of Nb- Zn doped Barium Strontium hexaferrite

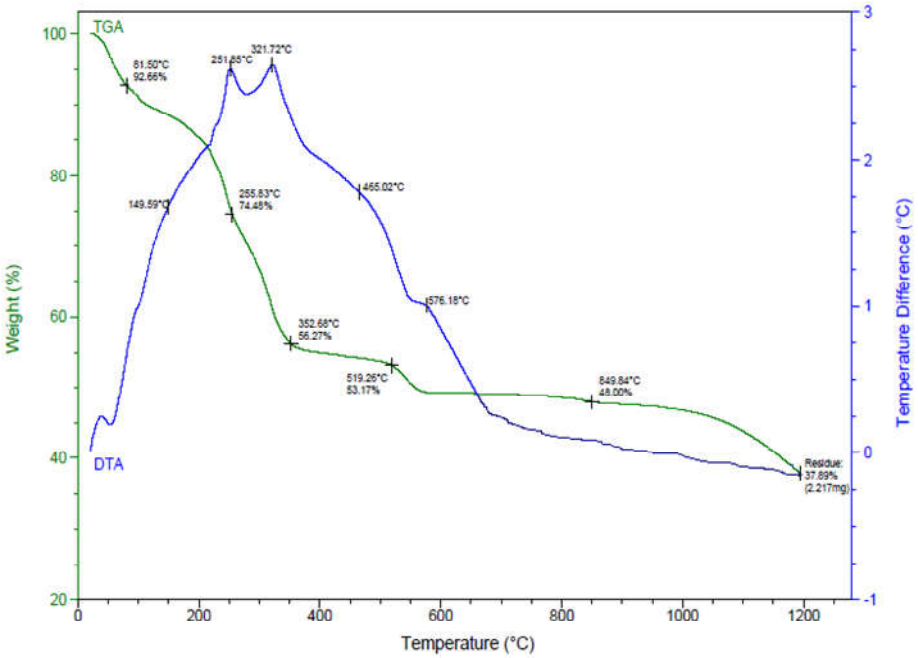

Fig. 2. TG/DTA curve for $Ba_{0.5}Sr_{0.5}Fe_{12}O_{19}$

Table 1. FTIR spectra of $Ba_{0.5}Sr_{0.5}Fe_{12-2x}Nb_xZn_xO_{19}$ precursors with (X=0, 0.05, 0.1, 0.25, 0.5 mol %)

Sample	weight percentage(cm^{-1})	vibrational mode(cm^{-1})
(G_1)$Ba_{0.5}Sr_{0.5}Fe_{12}O_{19}$	3451-3498	O – H Stretch
(G_2)$Ba_{0.5}Sr_{0.5}Fe_{11.9}Nb_{0.05}Zn_{0.05}O_{19}$	1704-1724	C = O Stretch
(G_3)$Ba_{0.5}Sr_{0.5}Fe_{11.8}Nb_{0.1}Zn_{0.1}O_{19}$	1353-1381	N = O Bend
(G_4)$Ba_{0.5}Sr_{0.5}Fe_{11.5}Nb_{0.25}Zn_{0.25}O_{19}$	1010-1065 , 797	C-O Stretch , Metal oxide
(G_5)$Ba_{0.5}Sr_{0.5}Fe_{11}Nb_{0.5}Zn_{0.5}O_{19}$	453-495	Ferrite

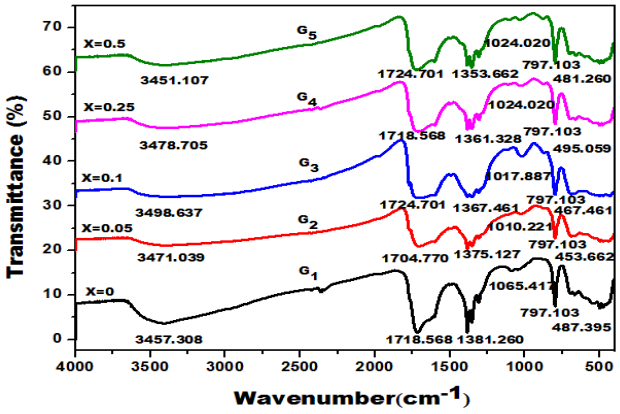

Fig. 3. FTIR spectra of $Ba_{0.5}Sr_{0.5}Fe_{12-2x}Nb_x Zn_xO_{19}$ precursors with (X=0, 0.05, 0.1, 0.25, 0.5 mol %)

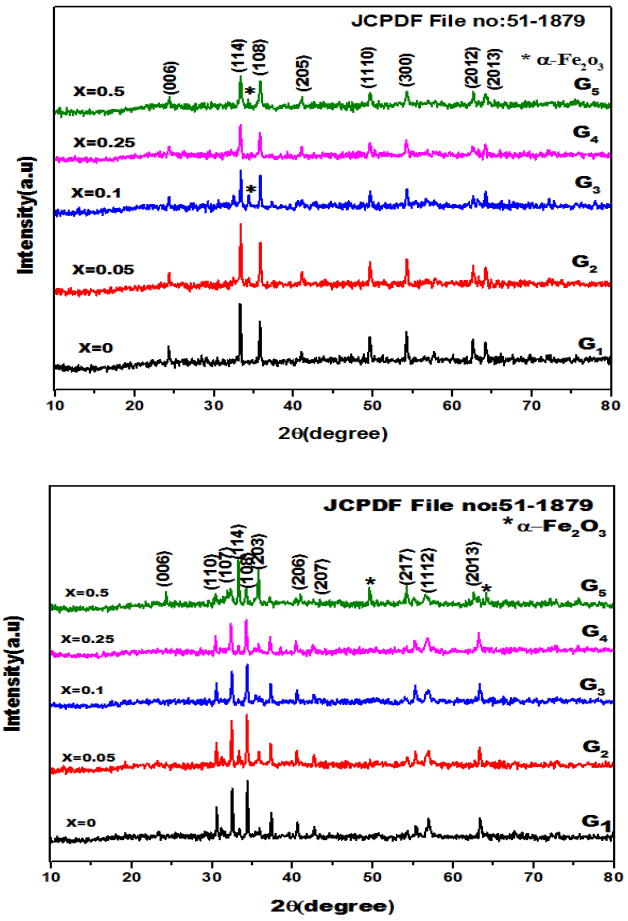

Fig. 4a. & 4b XRD patterns of the $Ba_{0.5}Sr_{0.5}Fe_{12-2x}Nb_xZn_xO_{19}$ (X=0, 0.05, 0.1, 0.25, 0.5 mol %)
Of samples calcined at (800^0C & 950^0C)

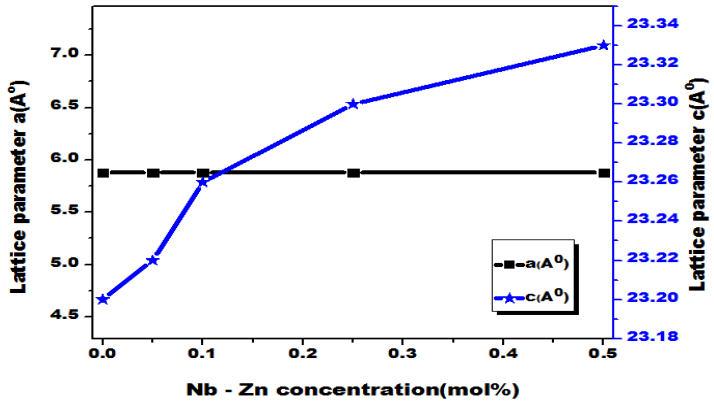

Fig. 5. Variation of lattice constants (a, c) with changes in the contents of Nb - Zn (x=0 – 0.5mol %)

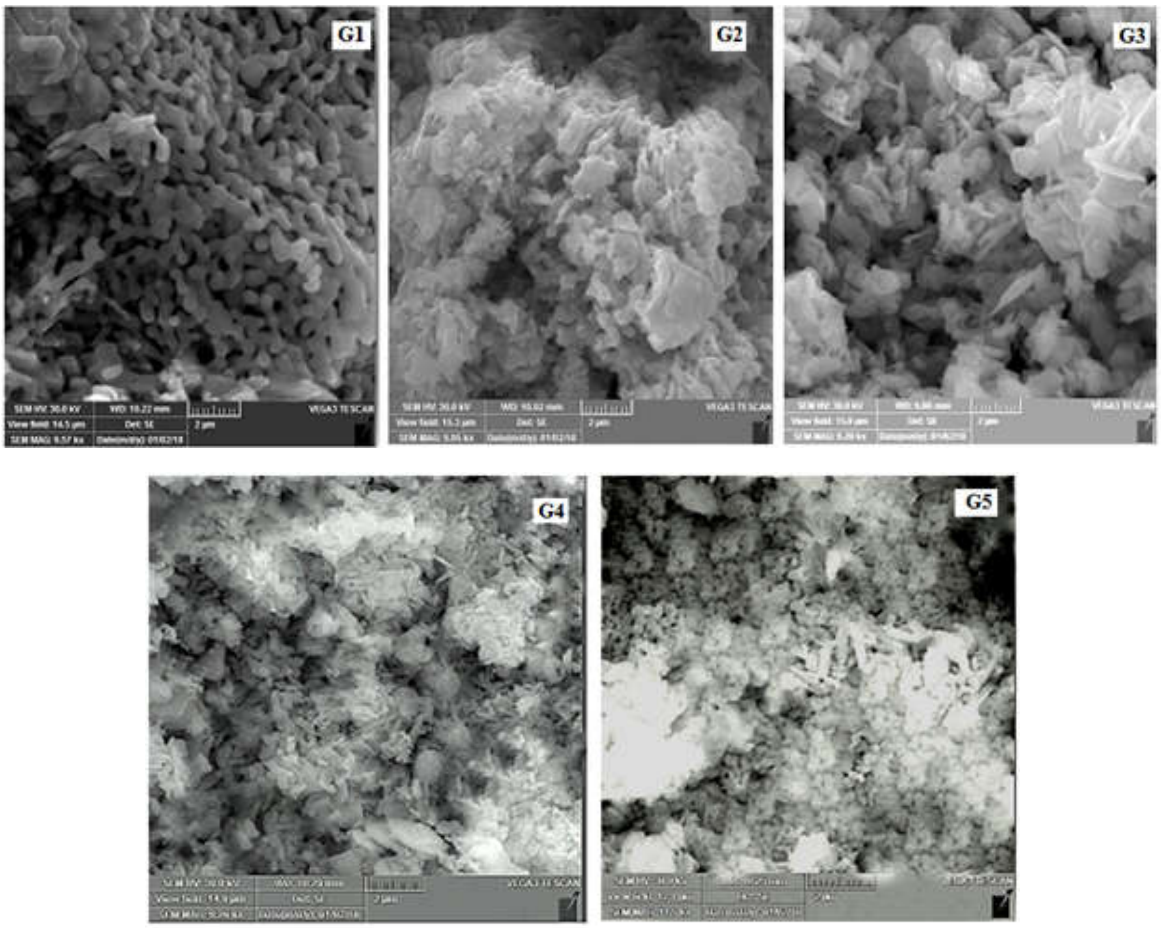

Fig. 6. SEM images of $Ba_{0.5}Sr_{0.5}Fe_{12-2x}Nb_xZn_xO_{19}$(X=0, 0.05, 0.1, 0.25, 0.5 mol %) with samples Calcined at 950^0C

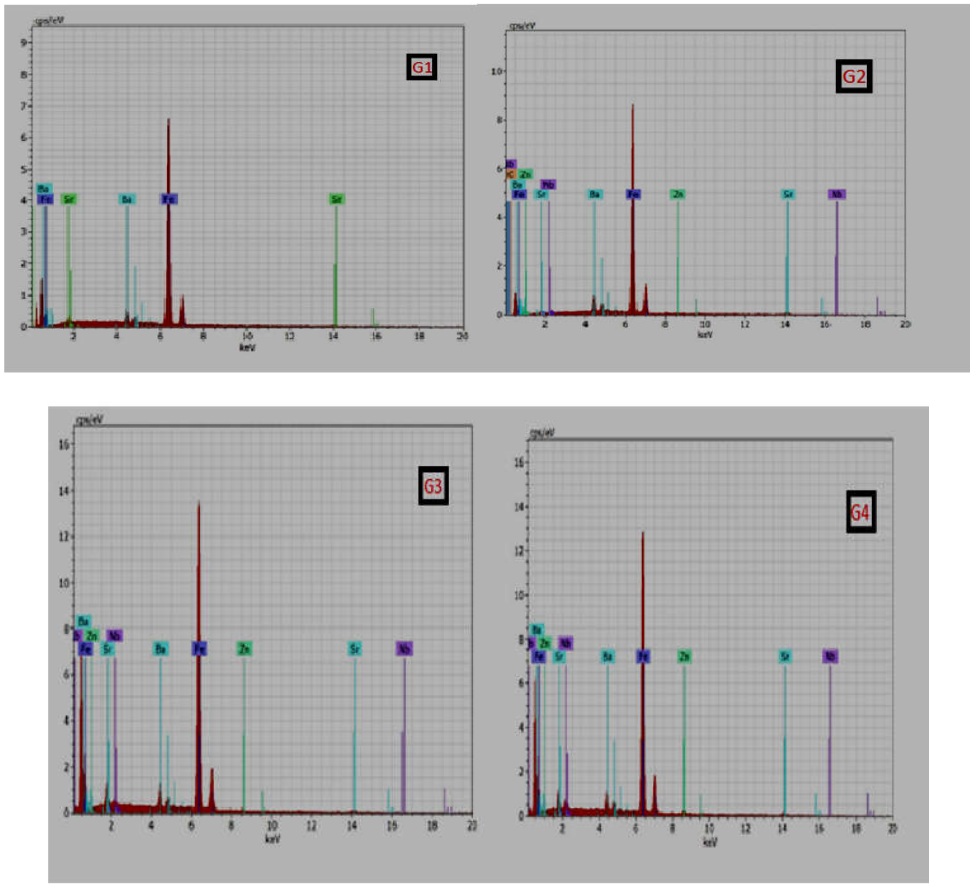

Continue…….

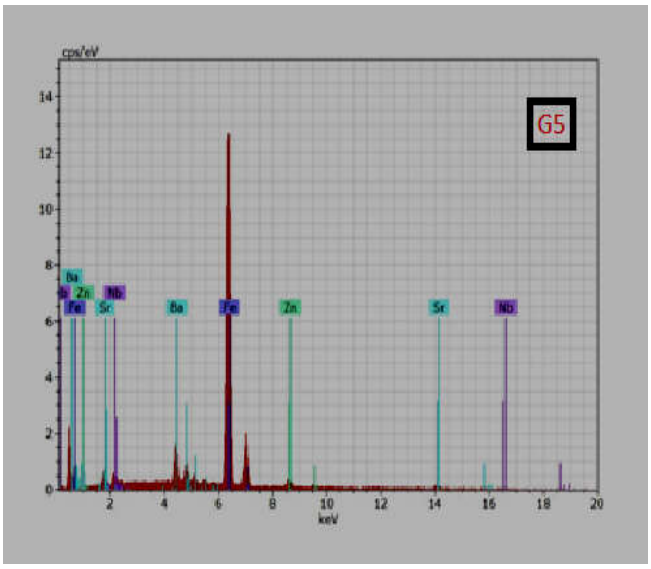

Fig.7 EDAX spectrum of $Ba_{0.5}Sr_{0.5}Fe_{12-2x}Nb_xZn_xO_{19}$(X=0, 0.05, 0.1, 0.25, 0.5 mol %) of samples calcined at 950^0C

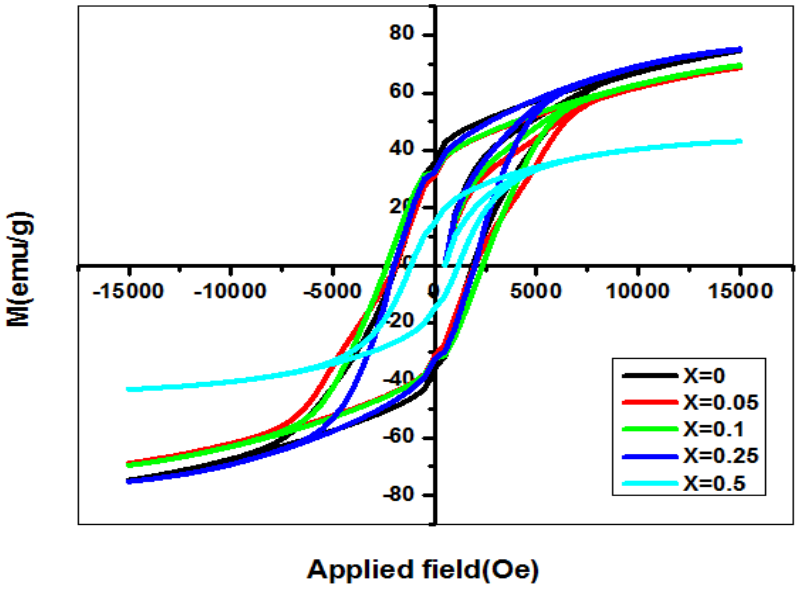

Fig. 8. Hysteresis loops of $Ba_{0.5}Sr_{0.5}Fe_{12-2x}Nb_xZn_xO_{19}$(X=0, 0.05, 0.1, 0.25, 0.5 mol %) at room temperature

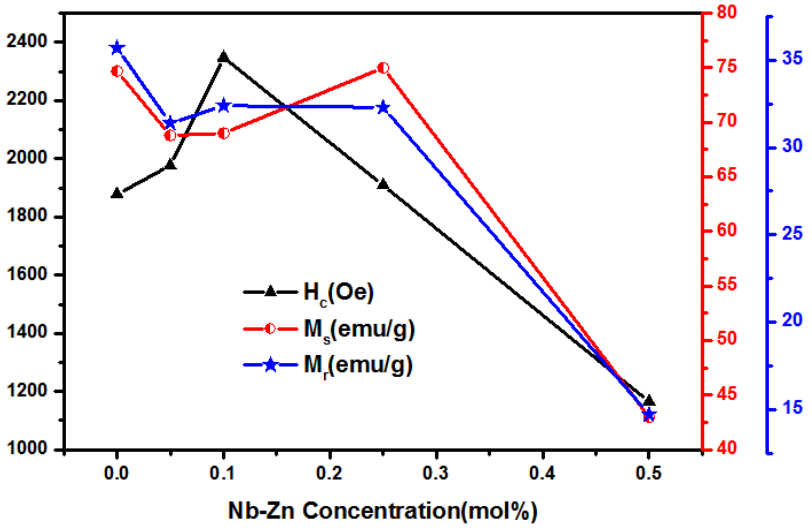

Fig.9 The saturation magnetization (Ms), the coercivity (Hc) and remanance magnetization (M_r) of samples $Ba_{0.5}Sr_{0.5}Fe_{12-2x}Nb_xZn_xO_{19}$(X=0, 0.05, 0.1, 0.25, 0.5 mol % at room temperature

$$\frac{1}{d_{hkl}^2} = \frac{4}{3}\left(\frac{h^2+hk+k^2}{a^2}\right) + \frac{l^2}{c^2} \quad (1)$$

Where d is the inter-planer spacing and values of 'h k l' are miller indices. The values of lattice parameter calculated using above equation (1). Variation of lattice parameters (a, c) as a function of Nb – Zn (X=0 to 0.5mol %) content is shown in fig 5. It is evident that the value of 'a' remains constant, while that of 'c' slightly increases with increasing the doping contents. The increase in lattice parameter c might have been caused by the difference between the ionic radii of Zn^{2+} ($0.74A^0$) and Nb^{4+} ($0.69A^0$) compared with that of Fe^{3+} ($0.645A^0$). The change in lattice parameters vary with the distance between magnetic ions which lead to a change in super exchange interactions and thus to a change in magnetic properties of the samples. This behavior was in good agreement with that of the previous work (Yujie Yang, 2014).

The particle size of the sample was calculated from Scherrer's formula (2)

$$D = k\lambda / \beta\cos\theta \quad \ldots\ldots\ldots(2)$$

Where D is the average crystallite size, λ is the X -ray wavelength (1.54060 A^0), β is the half peak width, θ is the Bragg's angle and k - shape factor (k = 0.89 for hexagonal system). The average crystallite size determined from XRD data is in the range of 31 - 48 nm, indicating the nanocomposition nature of the present samples.

Surface morphology analysis: The surface morphology and microstructure analysis of the samples have been investigated using SEM analysis. Fig 6 illustrates the typical SEM micrographs of hexaferrite $Ba_{0.5}Sr_{0.5}Fe_{12-2x}Nb_xZn_xO_{19}$ (X=0, 0.05, 0.1, 0.25, 0.5 mol %) samples at temperature, 950^0 C. The shape of the sample G_1 is the dumble shape, for the sample of G_2 and G_3 are in platelet hexagonal structure, whereas hexagonal with needle shape structure are found in the sample of G_4.The sample G_5 exhibited the shape of hexagonal along with tiny spherical particles which confirmed the presence of nanocomposite materials. The results of XRD and SEM are matched with each other. The platelet shaped hexaferrite can be used for microwave absorbing purpose (Kanagesan, 2012).

Energy dispersive X –ray spectroscopy: EDAX analysis of $Ba_{0.5}Sr_{0.5}Fe_{12-2x}Nb_xZn_xO_{19}$(X=0, 0.05, 0.1, 0.25, 0.5 mol %) of samples show the evidence for the presence of barium, strontium, iron, Niobium and Zinc.

Magnetic properties: Fig.8 shows the measured hysteresis loops for representative $Ba_{0.5}Sr_{0.5}Fe_{12-2x}Nb_xZn_xO_{19}$ samples as a function of applied magnetic field ±15KOe. The value of coercivity, saturation magnetization and remanence magnetization were observed from these loops. The estimated values of coercivity, saturation and remanence magnetization are shown in fig 9. It is clear from the figure that the saturation magnetization (M_s) increased from 74.7 emu/g at X=0 to 75.2 emu/g at X=0.25 and then slightly decreased at the value of 43.1 emu/g with the increase of doping content at X=0.5. The remanence magnetization decreased slightly from 35.7emu/g for the undoped sample at x=0 down to the 14.7emu/g for the doping level of X=0.5. The decrease in magnetization by further increase in Nb-Zn content could be related to the presence of α-Fe_2O_3 for X=0.5.

The value of coercivity first increases from 1877Oe at X=0 and reached the maximum value of 2348Oe at X=0.1 and then drops drastically at 1164Oe at x=0.5. The Nb-Zn doped with Ba-Sr hexaferrite with X up to 0.5 resulted in the reduction of coercivity and improved saturation and remanence magnetization at relatively high level suitable for high density magnetic recording applications. The Fe^{3+} ions in M-type hexaferrite structure are distributed on five different crystallographic sites such as three octahedral (2a, 12k and $4f_2$), one tetrahedral ($4f_1$) and one trigonal bipyramidal (2b) sites. In the magnetically ordered state in Ba-Sr hexaferrite, the 12k, 2a and 2b sites have their spins aligned parallel to each other in the crystallographic c-axis, but $4f_2$ and $4f_1$ sites point in the opposite direction (11). This is likely due to the site occupancy of the doped metal ions in the different lattice site substitution of the Fe^{3+} ions in the spin up states appears to cause reduction in magnetization while the substitution in the spin down states may lead to an increase in the net magnetization. The material with high coercivity can be used to high density perpendicular magnetic recording (32). In comparison of previous work, the coercivity is low but in the present work the coercivity is high. This reason is the benefit for the application.

Conclusion

M-type hexaferrite with compositions of $Ba_{0.5}Sr_{0.5}Fe_{12-2x}Nb_xZn_xO_{19}$ (X= 0, 0.05, 0.1, 0.25, 0.5 mol %) were successfully synthesized by sol-gel method using D-glucose as fuel. TGA/DTA curve showed there is no weight loss above 850^0C which confirming the formation of barium strontium hexaferrite. FTIR spectra showed the bands around 453 to 495 cm^{-1} which confirmed the presence of hexaferrite. XRD data of the synthesized samples confirmed the formation of hexagonal magnetoplumbite phase structures. The average crystallite size calculated from XRD is in the range of 31-48nm. The values of lattice parameter were calculated using interplaner spacing formula. SEM micrographs showed the powder is well crystallized and the particles are hexagonal structure with the needle shape and platelet form. The platelet shaped hexaferrite can be used for microwave absorbing purpose. XRD results are in good agreement with the SEM results. The EDAX indicated the presence of (Ba, Sr, Fe, Nb and Zn). The results show that the Nb-Zn doped with Ba-Sr hexaferrite with X up to 0.5 resulted in the reduction of coercivity and improved saturation magnetization and remanence magnetization at relatively high level suitable for high density perpendicular magnetic recording applications.

REFERENCES

Abbas, W., Ahmad, I., Kanwal, M., Murtaza, G., Ali, I. Khan, M.A., Akhtar, M.N., Ahmad, M. 2015. *J. Magn. Magn. Mater*. 374, PP.187–191.

Auwal, I.A., Güngünes, H., Baykal, A., Güner, S., Shirsath, S.E., Sertkol, M. 2016. *Ceram. Int*. 42, PP.8627– 8635.

Awadallah, A., Mahmood, S.H., Maswadeh, Y. Bsoul, I., Awawdeh, M., Mohaidat, Q.I., Juwhari, H. 2016. Mater. Res. Bull. 74, PP.192–201.

Buzinaro, M.A.P., Ferreira, N.S., Cunha, F., Macêdo, M.A. 2016. *Ceram. Int*. 42, PP.5865–5872.

Chavan, V.C., Shirsath, S.E., Mane, M.L., Kadam, R.H., More, S.S. 2016. *J. Magn. Magn. Mater*., 398,PP. 32–37.

Dhage, V.N., Mane, M.L., Babrekar, M.K., Kale, C.M., Jadhav, K.M. 2013. J. Alloys Compd. 509,PP. 4394–4398.

Ezhil Vizhi. R, Harikrishnan.V , Saravanan. P and Rajan Babu. D. 2016. *J. Cryst. Growth*. PP.1-22.

Fuzhan Song, Xiangqian Shen, Jun Xiang and Yongwei Zhu, 2010. *J. Alloys. Comp*. 507.PP. 297–301.

Jasbir Singh, Charanjeet Singh, Dalveer Kaur, S. Bindra Narang, Rajat Joshi, Sanjay Mishra, Rajshree Jotania, Madhav Ghimire and Chetna, C. 2016. Chauhan, *J. Mater. Design*.

Kanagesan, S., Hashima, M., Kalaivani, T., Ismaila, I., Rahmana, N. A. and Hajaliloua. A. 2014. *J.Chem. Pharm. Res.,* 6(4),PP.1210-1215.

Kanagesan, S., Jesurani, S., Velmurugan, R. and Kalaivani, T. 2010. *Trans. Ind. Ceram. Soc*., 69(3),PP.199-202.

Kanagesan, S., Jesurani, S., Velmurugan, R., Prabu, S. and Kalaivani, T. 2012. Mater. Res. Bull, 47, PP.188–192.

Kanagesan, S., Jesurani, S., Velmurugan, R., Prabu, S. and Kalaivani, T. 2012. *J Mater Sci:* Mater Electron. 23, PP. 1575– 1579.

Magn. Magn. Mater . 422,PP.209–215.

Marin Cernea, Simona-Gabriela Sandu, Carmen Galassi and Victor Kuncser, 2013. *J. Allo. Comp*. PP.1-29.

Mariño-Castellanos, P.A. 2004. J. Anglada-Rivera, A. Cruz-Fuentes, R. Lora-Serrano, *J. Magn. Magn. Mater*., 280, PP. 214–220.

Mocuta, H., Lechevallier, L., LeBreton, J.M., Wang, J.F., Harris, I.R. *J. Alloys Compd*. 364 PP.48–52.

Mozaffari, M., Arab, A., Yousefi, M.H.and Amighian, J. 2010. *J. Magn. Magn*. *Miater* .322, PP.2670–2674.

Muhammad Javed Iqbal and Saima Farooq, 2010. *J . Alloys Comp*. 505, PP. 560-567.

Pawar, P.A., Desai, S.S., Tamboli, Q.Y., Shirsath, S.E., Patange, M. 2015. *J. Magn. Magn. Mater*., 378,PP.59–63.

Safia Anjum, Sania Hameed, Saif Ullah Awan, Ejaz Amed, Abdul Sattar, 2016. *Int. J. Light and Electr. Optics*, PP.1-23.

Sami, H. 2017. Mahmood and Ibrahim Bsoul, Cond. *Mat. Mtrl. Sci.,* PP.1-47.

Samikannu Kanagesan, Mansor Hashim, Sinnapan Jesurani, Thirunavukarasu Kalaivani, Ismayadi Ismail, 2014. Mater. sci. Appl. 5, PP.171-176.

Silva, W.M.S., Ferreira, N.S., Soares, J.M., daSilva, R.B., Macêdo, M.A. 2015. *J. Magn.Magn. Mater.*, 395, PP. 263 –270.

Thakur, A., Singh, R.R., Barman, P.B. 2013. *J. Magn. Magn. Mater*. 326, PP. 35–40.

Trukhanov, A.V., Turchenko, V.O., Bobrikov, I.A., Trukhanov, S.V., Kazakevich, I.S., Balagurov, A.M. 2015. *J. Magn. Magn. Mater*. 393, PP.253–259.

Trukhanov, S.V., Trukhanov, A.V., Turchenko, V.A., Kostishin, V.G., Panina, L.V., Kazakevich, I.S., Balagurov, A.M. 2016. *J. Magn. Magn. Mater*. 417, PP. 130–136.

Wangchang Li,Xiaojing Qiao,Mingyu Li,Ting Liu and H.X, 2013. Peng, Mater. Res. Bull.48, PP.4449-4453.

Waseem Abbas, Ishtiaq Ahmad, M. Kanwal,GhulamMurtaza, Ihsan Ali, Muhammad Azhar Khan, Majid Nia zAkhtar and Mukhtar Ahmad, 2015. *J. Magn. Magn. Mater*. 374, PP.187–191.

Winataputra, D. S., Ujiyanti T. L. and Adi, W.A. 2017. Mater. Sci. Engi.202, 012090.

Yang Yujie, Wang Fanhou, Shao Juxiang, Huang Duohui and Cao Qilong. 2018. *Chinese. J. Phy*.56, PP.67–74.

Yujie Yang and Xian song Liu, J. Magn. Magn.Mater, 2014.

YujieYang, N., Fanhou Wang, Xiansong Liu, Juxiang Shao, Shuangjiu Feng, Duohui Huang and Mingling Li, 2017. J.

****